Published in final edited form as:

Metabolism. 2020 June ; 107: 154215. doi:10.1016/j.metabol.2020.154215.

Loss of *Ceacam1* promotes prostate cancer progression in *Pten* haploinsufficient male mice

Jehnan Liu[1,2], **Harrison T. Muturi**[1,2,3], **Saja S. Khuder**[1,2], **Raghd Abu Helal**[3], **Hilda E. Ghadieh**[1,2,3], **Sadeesh K. Ramakrishnan**[1,2], **Meenakshi K. Kaw**[1,2], **Sumona Ghosh Lester**[1,2], **Ahmed Al-Khudhair**[1,4], **Philip B. Conran**[5], **Khew-Voon Chin**[1,4], **Cara Gatto-Weis**[1,5], **Sonia M. Najjar**[1,2,3,6,†]

[1]Center for Diabetes and Endocrine Research at the University of Toledo College of Medicine and Life Sciences, Toledo, OH, 43614, USA

[2]Department of Physiology and Pharmacology at the University of Toledo College of Medicine and Life Sciences, Toledo, OH, 43614, USA

[3]Department of Biomedical Sciences, Heritage College of Osteopathic Medicine, Ohio University, Athens, OH, 45701, USA

[4]Department of Medicine at the University of Toledo College of Medicine and Life Sciences, Toledo, OH, 43614, USA

[5]Department of Pathology at the University of Toledo College of Medicine and Life Sciences, Toledo, OH, 43614, USA

[6]the Diabetes Institute, Heritage College of Osteopathic Medicine, Ohio University, Athens, OH, 45701, USA

Abstract

Objective: *PTEN* haploinsufficiency plays an important role in prostate cancer development in men. However, monoallelic deletion of *Pten* gene failed to induce high prostate intraepithelial neoplasia (PIN) until $Pten^{+/-}$ mice aged or fed a high-calorie diet. Because CEACAM1, a cell adhesion molecule with a potential tumor suppression activity, is induced in $Pten^{+/-}$ prostates, the study aimed at examining whether the rise of *Ceacam1* limited neoplastic progression in $Pten^{+/-}$ prostates.

[†]**Address correspondence to:** Sonia M. Najjar, Ph.D., Department of Biomedical Sciences, Heritage College of Osteopathic Medicine, Ohio University, Athens, Ohio, 45701, Tel: (740) 593-2376, FAX: (740) 593-2778, najjar@ohio.edu.

AUTHOR CONTRIBUTIONS

J.L., H.T.M., S.S.K., R.AH., H.E.G., S.K.R., M.K.K., S.G.L., and Al-K.A. researched and analyzed data; J.L. and K-V.C. drafted the article. H.T.M., S.S.K., H.E.G., R.AH., S.K.R., and C-G-W contributed to the editing of the manuscript. P.B.C. and C-G-W are certified pathologists that scored histology independently and contributed to data analysis. S.M.N. oversaw the work, including its conception and study design, analyzed data, led scientific discussions and reviewed/edited the manuscript.

CONFLICT OF INSTEREST

None declared

Methods: *Pten*$^{+/-}$ were crossbred with *Cc1*$^{-/-}$ mice harboring a null deletion of *Ceacam1* gene to produce *Pten*$^{+/-}$/*Cc1*$^{-/-}$ double mutants. Prostates from 7-month old male mice were analyzed histologically and biochemically for PIN progression.

Results: Deleting *Ceacam1* in *Pten*$^{+/-}$ mice caused an early development of high-grade PIN in parallel to hyperactivation of PI3 kinase/Akt and Ras/MAP kinase pathways, with an increase in cell proliferation, epithelial-to-mesenchymal transition, angiogenesis and inflammation relative to *Pten*$^{+/-}$ and *Cc1*$^{-/-}$ individual mutants. It also caused a remarkable increase in lipogenesis in prostate despite maintaining insulin sensitivity. Concomitant *Ceacam1* deletion with *Pten*$^{+/-}$ activated the IL-6/STAT3 signaling pathways to suppress *Irf-8* transcription that in turn, led to a decrease in the expression level of promyelocytic leukemia gene, a well characterized tumor suppressor in prostate.

Conclusions: *Ceacam1* deletion accelerated high-grade prostate intraepithelial neoplasia in *Pten* haploinsufficient mice while preserving insulin sensitivity. This demonstrated that the combined loss of *Ceacam1* and *Pten* advanced prostate cancer by increasing lipogenesis and modifying the STAT3-dependent inflammatory microenvironment of prostate.

Keywords

Prostate intraepithelial neoplasia; PTEN tumor suppression; CEACAM1; normoinsulinemia; Fatty acid synthase; Neoplasia; PML

1. INTRODUCTION

Recent surveys of the prostate cancer genome landscape by sequencing confirmed that prostate cancer harbors a wide array of recurrent genomic lesions encompassing gross chromosomal aberrations that include the frequent E26 transformation-specific (*ETS*) gene fusions, point mutations, and transcriptional and epigenetic changes [1]. These alterations consistently target the phosphatidylinositol 3-kinase genes (*PIK3CA* and *PIK3CB*) and the phosphatase and tensin homolog (*PTEN*) genes, among others. They also target a broad spectrum of frequent recurrent alterations of *TP53*, *FOXA1*, *KRAS* [2].

In addition, etiological and epidemiological data suggest that the subversion of inflammatory signals in response to extrinsic factors including environmental toxins and diet, enable the malignant transformation and progression of prostate cancer [3]. For instance, total loss of *PTEN* occurs in advanced prostate cancer with a Gleason score of ≥ 7 [4] and *PTEN* haploinsufficiency plays an important role in prostate cancer development [5]. However, monoallelic deletion of *Pten*, a significant recurrent prostate cancer gene [1, 6–9], fails to induce high prostatic intraepithelial neoplasia (PIN) until *Pten*$^{+/-}$ mice are older than 12 months [10, 11], or unless they are fed a high-calorie diet [12]. High-calorie diet accelerates prostate cancer progression in these insulin sensitive mice, owing to the rise in ectopic fat accumulation and associated pro-inflammatory microenvironment [12]. Biallelic deletion of *Pten* gene also led to minimally invasive prostate cancer with a long latency period [13, 14] that progressed to adenocarcinoma with additional deletions of JNK [15], Trp53 [16] and promyelocytic leukemia (PML) [17] genes.

The family of carcinoembryonic antigen related cell adhesion molecule (*CEACAM*) genes encode integral membrane glycoproteins that contain immunoglobulin domains-like structures with diverse cellular regulatory functions in cell adhesion, angiogenesis, metabolic regulation, immune response, proliferation, differentiation and tumor suppression/promotion [18]. The *CEACAM* gene family consists of 12 members that are localized in a single contiguous locus spanning approximately 10-Mbp on chromosome 19 [19]. Particularly, CEACAM1 appears to be repressed in prostate cancer cells [20] and in the early phases of hyperplastic lesions of prostate cancer [21, 22]. CEACAM1 expression in glandular epithelial cells decreases while it increases in endothelial cells during the "angiogenic switch" that occurs as prostate cancer progresses [23]. Nonetheless, the precise role of CEACAM1 in prostate cancer has not been fully addressed.

CEACAM1 plays a regulatory role in metabolism and immune response [24–26]. We and others have shown that its gene is alternatively spliced to encode a long (−4L) and a short (−4S) isoforms differing by the loss of a 61 amino acid-sequence from the intracellular tail of the short isoform that contains key serine and tyrosine phosphorylation sites [25, 26]. Upon its phosphorylation by insulin receptor, CEACAM1 induces the rate of insulin-mediated receptor uptake and degradation. Whether it promotes renal C-peptide clearance is not known, but deletion or functional inactivation of *Ceacam1* in mice impairs insulin clearance to cause systemic insulin resistance and metabolic dysregulation, including visceral obesity with its associated pro-inflammatory microenvironment [24, 27–29].

CEACAM1 is phosphorylated by insulin and epidermal growth factor (EGF) receptors, but not by the insulin-like growth factor-1 (IGF-1) receptor [30, 31]. When phosphorylated, it sequesters Shc to limit coupling of the Ras/MAPK to the receptors and restrict cell proliferation in response to insulin and EGF [30, 31].

CEACAM1 protein level is elevated in prostates of 7-month old $Pten^{+/-}$ mice with a low PIN [12], resulting from hyperactivated Akt-SOX9 pathway [32] and intact response to insulin [33]. Thus, we herein investigated whether the increase in CEACAM1 expression contributed to the restricted neoplastic effect of *Pten* haploinsufficiency in mice by testing whether concomitant *Ceacam1* deletion promotes high-grade prostate intraepithelial neoplasia (PIN) in $Pten^{+/-}$ mice, and whether this is associated with altered metabolism.

2. MATERIALS AND METHODS

2.1 Mouse models

C57BL/6J.129-$Pten^{tm1Rps}$ mice ($Pten^{+/-}$) were obtained from the National Cancer Institute's Mouse Models of Human Cancers Consortium (MMHCC) [10] and C57BL/6J.$Cc1^{-/-}$ mice from the Beauchemin laboratory [34]. $Pten^{+/-}$ were crossbred with $Cc1^{-/-}$ mice to produce offsprings harboring several genotypes that include $Pten^{+/+}/Cc1^{+/+}$ ($Pten^{+/+}$ or wild-type), $Pten^{+/-}$, $Cc1^{-/-}$, and $Pten^{+/-}/Cc1^{-/-}$ mice. Mice were kept in a 12hr-light/dark cycle in pathogen-free conditions and fed *ad libitum* a standard chow diet. Animal studies were performed on 7-month old male mice per the guidelines of the Institutional Animal Care and Utilization Committee at the University of Toledo.

2.2 Biochemical parameters

Mice were fasted overnight, anesthetized with sodium pentobarbital (55 mg/kg body weight) and their whole venous blood drawn from retro-orbital sinuses at 11:00 a.m. to measure steady-state fasting glucose levels using a glucometer (Accu-chek® Aviva; Roche® Diagnostics, Indianapolis, IN), plasma insulin and C-peptide levels by a radioimmunoassay (Millipore, St. Charles, MO), non-esterified fatty acids (NEFA) by NEFA C kit (Wako Diagnostics, Richmond, VA), triglycerides by a kit from Pointe Scientific (Canton, MI), and cholesterol and testosterone by kits from Endocrine Technologies (Newark, CA). Visceral white adipose tissue (gonadal plus inguinal), prostates and other tissues were removed, weighed, fixed or frozen for further analysis.

2.3 Histopathology

Prostate ventral and dorsolateral lobes were formalin-fixed, paraffin-embedded and serially sectioned to 5 μm thickness [12]. Some sections were stained with Hematoxylin & Eosin (H&E) and analyzed for PIN. Two expert pathologists assigned PIN stage based on the most severe lesion found on a single H&E slide [35]. Normal prostate glands have a thin myoepithelial layer and a continuous lining of cuboidal epithelium with basal nuclear polarity; PIN-I has 1 or 2 layers of atypical luminal cells; PIN-II has 3 or more layers of atypical cells and glands have flatter luminal edges with occasional crowding, infolding and tufting of epithelium. PIN-III has atypical luminal cells with extensive gland-in-gland proliferation almost filling the entire lumen characterized by pleomorphic nuclei and prominent nucleoli, and PIN-IV fills and expands the glandular lumen, distorting the glandular profile. Although PIN-IV lesions can be large and show cellular pleomorphism, they can be differentiated from adenocarcinomas by the lack of invasion of the basement membrane surrounding the gland with necrotic debris and inflammatory cells at the site of invasion.

2.4 Immunohistochemistry

Antigen was retrieved in rehydrated sections using antigen retrieval solution (Vector Laboratories Inc., Burlingame, CA) [12]. Briefly, sections were incubated overnight at 4°C in primary antibodies diluted in MOM diluent, using VECTASTAIN Elite ABC PERXIDASE kit PK-6101 and vector MOM immunodetection PEROXIDASE kit PK-2000 (Vector laboratories, Burlingame, CA). The antibodies included: α-Ki67 (monoclonal, BD Pharmingen, NJ, USA), α-FASN (polyclonal, Enzo Life Sciences, Plymouth Meeting, PA), α-SOX9 (polyclonal, Santa Cruz Biotech, Santa Cruz, CA), α-SNAIL (polyclonal, Abcam, Cambridge, MA), α-E-Cadherin (monoclonal, Cell Marque Rocklin, CA), F4/80 (polyclonal, Abcam), FoxP3 (polyclonal, Abcam), CD4 (monoclonal, Abcam), CD8 (monoclonal, Lifespan Biosciences, Seattle, WA) and Gr1 (Ly6C+ monoclonal, BD Biosciences, San Jose, CA). Secondary antibodies were then added, and sections were washed with the Vector® NovaREDTM Substrate Kit SK-4800 and DAB Peroxidase Substrate Kit SK-4100 (Victor Laboratories), per manufacturer's instructions.

2.5 Western blot

Prostate anterior lobes were lysed and their protein concentrations determined by BCA protein assay (Pierce, Waltham, MA) prior to analysis by 4–12% (Invitrogen, Waltham, MA) or 7%SDS-PAGE gels. Immunoblotting was performed using the following antibodies: polyclonal antibodies raised in rabbit against mouse CEACAM1 (Ab-2457 custom-made rabbit polyclonal), α-phospho-p44/42 (pMAPK), α-p44/42 (MAPK), α-phosphoSer 473-Akt, α-Akt, α-phosphoTyr1173-EGFR, α-EGFR, α-phosphoTyr705-Stat3, α-Stat3 (Cell signaling, Danvers, MA, USA), PTEN (Cascade Biosciences, Winchester, MA) and PML (Novus Biologicals, Littleton, CO). Depending on the apparent molecular mass, membranes were cut in half to probe the lower half with monoclonal antibody against GAPDH (Santa Cruz Biotech) to normalize for total protein content. For signaling gels, 2 parallel gels were applied to probe one with anti-phosphoantibodies and the other one with an antibody against the target protein. Proteins were detected using LiCOR secondary antibodies (LiCOR Biosciences, Lincoln, BE) and enhanced chemiluminescence (GE Healthcare Life Sciences, Amersham, Sunnyvale, CA) [12], and densitometry analysis was performed using Image J and calculated as percentage of the amounts of proteins loaded. Due to limited prostate tissue/mouse, different set of mice were used to analyze different proteins.

2.6 Semi-quantitative real-time RT-PCR

Total RNA was extracted from the anterior lobe of prostate using PerfectPure RNA Tissue Kit (5 Prime, Gaithersburg, MD) per manufacturer's instructions. One μg of RNA was reverse-transcribed using iScript™ cDNA synthesis kit (Bio-Rad Laboratories, Herculus, CA), and mRNA level of individual genes was analyzed by semi-quantitative real-time PCR (qRT-PCR) (Step One Plus Real time PCR system, Applied Biosystems, Foster City, CA) using gene-specific primers (Table S1), and normalized against 18S mRNA.

2.7 Statistical analysis

Because samples per each genotype were randomized irrespective of PIN lesions, data were analyzed by one-way analysis of variance (ANOVA) using Tukey's test for multiple comparison. Statistical analysis was performed using GraphPad Prism software. $P<0.05$ were statistically significant.

3. RESULTS

3.1 Loss of CEACAM1 advances prostate cancer in *Pten*$^{+/-}$ mice

As expected [12], Western blot analysis (Figure 1A.*a*) revealed a significant increase in CEACAM1 protein levels in prostates of *Pten*$^{+/-}$ relative to wild-types, resulting from increased SOX9 activation and enhanced insulin signaling [12]. qRT-PCR analysis showed that this involves a ~2-fold increase in the 4L long without affecting the 4S short isoform (Figure 1A.*a*). Because CEACAM1–4L may suppress tumor in experimental models of prostate cancer [19, 20], we tested whether the increase in CEACAM1 expression contributed to the restricted prostate cancer in *Pten*$^{+/-}$ mice by examining whether ablating *Ceacam1* gene advances their neoplasia. H&E stained sections of prostates of 7-month old wild-type and *Cc1*$^{-/-}$ null mice showed comparably low-grade PIN 0-I (Table 1, 33% and

46%, respectively; Figure 1B, hollow red arrow) and PIN-II (Table 1, 58% and 50% respectively; Figure 1B, hollow black arrow) with relatively few PIN-III (Table 1, 8% and 4% respectively; Figure 1B, solid red arrow) but no PIN-IV lesions (Table 1). In contrast, prostates from *Pten*$^{+/-}$ mutants showed predominantly PIN-III penetrance with gland-in-gland proliferation inside the lumen (Table 1, 69%, Figure 1B, solid red arrow). *Pten*$^{+/-}$/*Cc1*$^{-/-}$ mice showed more progressive PIN-III lesions with a ~2-fold increase in PIN-IV penetrance [more complex glandular proliferation (Figure 1B, solid black arrowhead) with carcinoma in situ (Figure 1B, solid black arrow)] and a diffuse stromal invasion (Figure 1B, hollow black arrowhead and Table 1, 10%). This demonstrates that ablating *Ceacam1* enhanced the penetrance and induced the progression of prostate cancer in *Pten* haplodeficient mice. Consistent with metastatic disease in humans [36], this was accompanied by markedly lower plasma testosterone levels in the *Pten*$^{+/-}$/*Cc1*$^{-/-}$ double mutants relative to the other groups of mice (Figure 2K).

3.2 Increased epithelial cell proliferation in prostates of *Pten*$^{+/-}$/*Cc1*$^{-/-}$ mice

Being a dual specificity protein phosphatase that catalyzes the dephosphorylation of membrane phospholipids, loss of PTEN is associated with hyperactivation of the phosphoinositide 3-kinase-Akt (PI3K/Akt) and the mitogen-activated protein kinase (MAPK) signaling networks that are implicated in prostate tumorigenesis [37]. Moreover, upon its phosphorylation, CEACAM1–4L binds to and sequesters Shc, leading to its reduced coupling of Ras-MAPK to insulin and EGF receptors [30, 31]. Accordingly, immunoblotting analysis of prostate lysates with α-phosphoAkt and α-phospho42/44 antibodies revealed an increase in Akt and MAPK phophorylation in individual knockouts, respectively, but more strongly in *Pten*$^{+/-}$/*Cc1*$^{-/-}$ double mutants without affecting basal EGFR phosphorylation (Figure 3A). In *Pten*$^{+/-}$ and *Pten*$^{+/-}$/*Cc1*$^{-/-}$ mutants, immunohistochemical (IHC) analysis (Figure 3B) showed a mild, but a significant increase in the expression of SOX9, an Akt downstream target that promotes luminal cell proliferation and early high-grade PIN lesions in mice [38]. As PIN progressed, SOX9 immunostaining increased in nuclei (Figure 3B, arrow), but especially in the cytoplasm of *Pten*$^{+/-}$/*Cc1*$^{-/-}$ double mutants (Figure 3B, arrowhead) where its mRNA level was ~2-fold higher than *Pten*$^{+/-}$ mutants (Table 2). In contrast, *Cc1*$^{-/-}$ mice manifested no increase in SOX9 mRNA levels (Table 2) or positive cells (Figure 3B). Consistently, mRNA levels of β-catenin proto-oncogene, another downstream target of Akt, were 4- and 13-fold higher in *Pten*$^{+/-}$ and *Pten*$^{+/-}$/*Cc1*$^{-/-}$ mice, respectively, relative to wild-types and *Cc1*$^{-/-}$ individual mutants. Similarly, mRNA levels of Cyclin D and p21, which mediate Akt-dependent cell survival pathways [39], increased significantly in *Pten* mutants, in particular in *Pten*$^{+/-}$/*Cc1*$^{-/-}$ double knockouts where p21 increased by ~40-fold, but not in *Cc1*$^{-/-}$ individual mutants that manifested normal levels (Table 2). Taken together, this demonstrates that *Cc1*$^{-/-}$ ablation further activated the Akt-dependent cell survival cascade in *Pten*$^{+/-}$ prostates. In concert with enhanced MAPK-pathways, this induced cell proliferation in *Pten*$^{+/-}$/*Cc1*$^{-/-}$ relative to *Pten*$^{+/-}$ prostates, as demonstrated by the ~2-fold increase in *Igf-1* mRNA levels (Table 2) and the Ki67 staining in prostate sections of the double mutants (Figure 3C), without any significant change in cell proliferation in *Cc1*$^{-/-}$ (Figure 3C).

3.3 Elevated epithelial-to-mesenchymal transition in *Pten*$^{+/-}$/*Cc1*$^{-/-}$ prostates

Consistent with induced levels of SNAIL during epithelial-to-mesenchymal transition (EMT); an event that promotes cellular invasiveness and metastatic spread [40], IHC analysis indicated a significant increase in SNAIL expression in cells in the stroma, around capillaries and within the glands in *Pten*$^{+/-}$/*Cc1*$^{-/-}$ relative to other groups of mice (Figure 4A). This was accompanied by a prominent loss of E-cadherin in *Pten*$^{+/-}$/*Cc1*$^{-/-}$ double mutants (Figure 4B), as expected from the repression of E-cadherin by SNAIL [40]. The higher MAPK activation in the double mutants is likely to mediate their superior EMT transition relative to *Pten*$^{+/-}$ heterozygous mice.

Like many other cancers, advanced prostate cancer exhibits an increase in angiogenesis. Accordingly, IHC analysis showed a remarkable induction in the expression level of CD31 (not shown) and VEGFR2 in *Pten*$^{+/-}$/*Cc1*$^{-/-}$ mutants (Figure 4C), consistent with the role of this pro-angiogenic tyrosine kinase receptor in EMT in advanced prostate cancer [41]. *Pten* haploinsufficient mice exhibited an increase in the mRNA levels of factors involved in regulating endothelial and vascular integrity, such as angiopoietin1 (*Ang1*) and *Hif1α* (Table 2, *Pten*$^{+/-}$ vs wild-types), the latter resulting from Akt hyperactivation and constituting an early event in prostate carcinogenesis, as we have previously shown [12]. Consistent with advanced metastatic lesions, the mRNA levels of these pro-angiogenic factors were further induced by ~2–3 fold by concomitant *Ceacam1* deletion (Table 2, *Pten*$^{+/-}$/*Cc1*$^{-/-}$ vs *Pten* $^{+/-}$). These factors were not significantly altered in *Cc1*$^{-/-}$ prostates (Table 2).

3.4 Elevated lipogenic gene expression in *Pten*$^{+/-}$/*Cc1*$^{-/-}$ mice

De novo fatty acid synthesis provides a key energy source for cancer cells to proliferate [42]. As Table 2 shows, mRNA levels of peroxisome proliferator-activated receptor γ (PPARγ) and sterol regulatory element binding proteins (SREBP-1c) were elevated in *Pten*$^{+/-}$, but not *Cc1*$^{-/-}$ mice (Table 2), as we [12] and others [17] have shown. Concomitant *Ceacam1* deletion further induced these mRNAs by ~2-fold (Table 2, *Pten*$^{+/-}$/*Cc1*$^{-/-}$ vs *Pten*$^{+/-}$). Consistent with SREBP-1c being a master transcriptional regulator of lipogenic genes, fatty acid synthase (FASN) protein levels were remarkably induced in *Pten*$^{+/-}$/*Cc1*$^{-/-}$ vs *Pten*$^{+/-}$ mice, as shown by IHC analysis (Figure 4D) and as shown in high-grade human prostate cancer [43, 44].

The increase in FASN protein level in *Pten*$^{+/-}$/*Cc1*$^{-/-}$ prostates was not accompanied by significant metabolic abnormalities (Figure 2). Contrary to impaired insulin clearance, as assessed by lower steady-state C-peptide/insulin molar ratio (Figure 2F), and the resulting chronic fasting hyperinsulinemia in *Cc1*$^{-/-}$ nulls (Figure 2D), *Pten*$^{+/-}$ and *Pten*$^{+/-}$/*Cc1*$^{-/-}$ mice exhibited normal insulin clearance and ensuing normo-insulinemia, proposing insulin sensitivity in these *Pten* mutants. In contrast to *Cc1*$^{-/-}$, *Pten*$^{+/-}$/*Cc1*$^{-/-}$ double mutants did not manifest an increase in body weight (Figure 2A), visceral obesity (Figure 2B), plasma NEFA (Figure 2C), or fed blood glucose levels (Figure 2H). This suggests that the insulin sensitivity state that was caused by the monoallelic deletion of *Pten* [45] reversed insulin resistance resulting from the total loss of *Ceacam1* [28] (herein manifested by fasting hyperinsulinemia and postprandial hyperglycemia). As observed previously [12, 46], fasting blood glucose, plasma triglycerides and cholesterol levels were normal in *Cc1*$^{-/-}$ individual

mutants. These metabolic parameters were not altered by the combined loss of *Pten* (Figures 2G, 2I, 2J, respectively).

3.5 Enhanced inflammation in *Pten*$^{+/-}$/*Cc1*$^{-/-}$ prostates

Targeted *Pten* inactivation in mice elevates inflammatory response [47], and CEACAM1 regulates inflammation in cancer [48]. Accordingly, IHC analysis showed that prostate sections derived from *Pten*$^{+/-}$/*Cc1*$^{-/-}$ double mutants exhibited a remarkable increase in multiple foci of stromal mononuclear inflammatory infiltrates such as macrophages (F4/80), T-cells (CD4/CD8), T-regulatory cells (FoxP3), and inflammatory monocytes (Gr1), compared to wild-type and single *Pten*$^{+/-}$ and *Cc1*$^{-/-}$ mutants (Figure 5, circles). This was further supported by qRT-PCR analysis showing an increase in the mRNA levels of several cytokines and chemokines, including: *Tnfa*, *Cd3*, *Cd45*, *Foxp3* (Table 2), *Il6*, *Gr1 (Ly6G+)*, *Cd11b* and *Ccl2* (Figure 6A) in the double relative to each individual mutant and wild-type groups. The mRNA levels of the granulocyte [Gr1(Ly6G+)] and the macrophage (Cd11b) markers (Figure 6A) were also elevated by 2-to-3-fold in *Pten*$^{+/-}$/*Cc1*$^{-/-}$ prostates (Figure 6A), likely resulting from the marked reduction (~5-fold) in the mRNA of interferon regulatory factor-8 (*Irf-8*) (Figure 6A), which is mostly expressed in cells of myeloid and lymphoid lineages, predominantly monocytes/macrophages. Reduction in *Irf-8* of *Pten*$^{+/-}$/*Cc1*$^{-/-}$ prostates could likely result from IL-6 activation of STAT3 pathway [49], as supported by the ~4-fold increase in *Il-6* mRNA (Figure 6A) and in their more robust STAT3 phosphorylation than individual mutants (Figure 6B).

Additionally, activation of STAT3 and downregulation of *Irf-8* reduce the transcription of *Pml* [50], a well characterized tumor suppressor gene that is concomitantly lost with PTEN in metastatic prostate cancer in humans [17]. Consistently, mRNA (Figure 6A) and protein (Figure 6B) levels of PML were lower in the prostates of *Pten*$^{+/-}$/*Cc1*$^{-/-}$ than the other groups of mice.

4. DISCUSSION

Recent advances in genomic sequencing have led to the identification of a number of genetic alterations in prostate cancer [1]. Overall, primary and metastatic tumors showed various combinations of modifications in oncogenes and tumor suppressor genes. These observations prompted the identification of partner genes in prostate tumorigenesis to better understand the pathogenesis of the disease [1, 6–9].

Although *PTEN* is one of the most frequently and recurrently mutated genes in prostate cancer in men [1], most studies have shown that partial or total loss of *Pten* alone does not drive metastatic carcinoma in mice, and that additional genetic changes must accrue to mediate prostate cancer progression [10, 11, 13, 14, 51]. The current study demonstrated that ablating *Ceacam1* in *Pten*$^{+/-}$ mice accelerated the progression of high-grade PIN lesions in parallel to inducing FASN and activating STAT3-dependent mechanisms without causing systemic insulin resistance. In contrast, its individual deletion caused low-grade PIN with insulin resistance. This demonstrates that multiple synergistic genomic alterations are required to drive tumor progression in prostate, mediated chiefly by lipogenesis and inflammation, as has been shown in human prostate cancer cells and in genetically

predisposed mice [43, 44, 52]. Moreover, this validates the emerging use of FASN inhibitors, such as orlistat, to limit progression of prostate cancer in men [44].

That total loss of *Ceacam1* exhibits a cooperative effect with monoallelic deletion of *Pten* to cause progression of prostate cancer is consistent with the mechanistic action of CEACAM1 in suppressing cell proliferation and cell adhesion [25, 30, 31]. The mechanism of CEACAM1-mediated growth inhibition is commonly attributed to its alternative spliced long isoform [53], which has a cytoplasmic tyrosine phosphorylation site within a conserved immunoreceptor tyrosine-based inhibitory motif (ITIM) domain that interacts with Src homology 2 domain (SH2)-containing tyrosine phosphatases to terminate growth signaling by tyrosine kinases [54]. Upon its phosphorylation by EGF [31] and insulin [30] receptors, CEACAM1–4L binds to Shc to sequester it and decrease coupling of the ras-MAPK pathway to the receptors, limiting the mitogenic functions of these growth factors. In fact, transgenic mice with liver-specific inactivation of CEACAM1 harboring a phosphorylation-defective dominant-negative mutant exhibited higher basal activation of MAPK resulting from increased Shc coupling to EGFR [31]. Thus, combined with increased Akt activation by partial loss of *Pten*, elevated MAPK activity caused by the absence of CEACAM1's sequestration of Shc caused a more robust cell proliferation and survival of prostate in the insulin sensitive $Pten^{+/-}/Cc1^{-/-}$ relative to the insulin resistant $Cc1^{-/-}$ mutants. In this regard, SiRNA-mediated downregulation of PTEN increased cell growth and soft agar clonicity in response to insulin in RWPE-1 normal human prostatic cells [12]. Of interest, increased cell proliferation occurred in parallel to elevation in FASN expression. Based on blunted proliferative effect of insulin in RWPE-1 normal prostate cells when FASN was downregulated in addition to PTEN [12], it is reasonable to assign a critical role for elevated FASN level in the neoplastic transformation of $Pten^{+/-}/Cc1^{-/-}$ prostates. This notion is supported by the positive role of PPARγ/FASN-driven lipogenesis (together with PI3K/AKT activation) in metastatic prostate cancer in men [52] and in high-fat diet-fed *Pten/Pml* mutant mice [17].

Like *Ceacam1*, the concomitant loss of *Pml* tumor suppressor gene with *Pten* caused metastatic prostate cancer in mice [17]. Interestingly, the progressive phenotype in $Pten^{+/-}/Cc1^{-/-}$ prostates was associated with a marked decrease in mRNA and protein levels of PML. The reduction of *Pml* transcript in $Pten^{+/-}$ prostates by concomitantly deleting *Ceacam1* appears to result from the activation of the IL-6/STAT3 pathway that in turn, inhibits *Irf-8* transcription to repress *Pml* [50].

Suppressing *Irf-8* could also induce the pool of granulocyte [Gr1(Ly6G+)] and macrophage (Cd11b) markers that are co-expressed uniquely on the surface of the myeloid-derived suppressor cells [49], likely contributing to the invasiveness in $Pten^{+/-}/Cc1^{-/-}$ prostates.

Activation of STAT3 and its transcriptional target, CCL2/MCP1 [55], upon *Ceacam1* deletion is consistent with the reported negative effect of CEACAM1-L overexpression on STAT3/CCL2 pathway in metastatic MC38 mouse cells [53]. Given that CCL2 induces the recruitment of M2-like tumor-associated macrophages and T-regulatory cells to promote metastasis [56], this assigns a significant role for this myeloid-associated chemokine in the progressive prostate cancer in $Pten^{+/-}/Cc1^{-/-}$ relative to individual mutants.

The remarkable increase in IL-6 levels caused by *Ceacam1* deletion particularly when combined with *Pten* haplodeletion could result from altered regulation of IL-6 production by CEACAM1 in monocytes [57]. Nonetheless, the dramatic increase of this cytokine in the prostates of $Pten^{+/-}/Cc1^{-/-}$ double mutants compared to controls is consistent with its role in prostate cancer progression [58] and its synergistic effect with insulin in inducing cell growth in human RWPE-1 cells with SiRNA-mediated downregulation of PTEN [12]. Together with the superior increase in other inflammatory markers such as Foxp3+Treg pool which correlates with advanced tumor [59], the data suggest that changes of the inflammatory microenvironment caused by *Ceacam1* deletion contributed to the neoplastic progression in $Pten^{+/-}/Cc1^{-/-}$ double mutants.

Although CEACAM1 is involved in angiogenesis, tumor progression and invasion [19, 48, 60], loss of *Ceacam1* worked in concert with the loss of *Pten* to promote prostate cancer progression and metastasis, consistent with lower expression of both genes in human prostate cancer [4, 43]. The underlying mechanisms implicate the activation of the IL-6/STAT3 signaling pathways that suppress *Irf-8* transcription followed by repression of PML tumor suppressor gene, as summarized in Figure 7.

5. STRENGTHS AND WEAKNESSES

The current studies provide an *in vivo* demonstration of how *Ceacam1* loss accelerates the oncogenic effect of *Pten* haplodeletion. This supports the merit of establishing the combined loss of CEACAM1 and PTEN as hallmark biomarkers in the progression of human prostate cancer. Clinical studies are needed to identify whether the loss of both genes occurs in patients with advanced Gleason score and whether targeting both genes would constitute better therapeutic strategies than those currently used.

6. CONCLUSIONS

The current studies show that *Ceacam1* deletion synergizes with that of *Pten* to drive the tumorigenic progression of high-grade PIN in mice. This appears to be mediated, at least in part, by increased lipogenesis and changes in the STAT3-dependent inflammatory microenvironment of prostate.

Supplementary Material

Refer to Web version on PubMed Central for supplementary material.

ACKNOWLEDGMENTS

The authors thank Melissa Kopfman at the Najjar laboratory for excellent technical assistance. They also thank Dr. Sadik A. Khuder from the University of Toledo, for invaluable help in statistical analysis. Special thanks to the Frederick W. Hiss endowment fund at the University of Toledo and the Osteopathic Heritage Foundation for the John J. Kopchick, PhD, Eminent Research Chair fund at Ohio University to S.M.N.

This work was supported by NIH grants: R01-DK054254, R01-DK083850, and R01-HL112248 to S.M.N. The work was also supported by the Middle-East Diabetes Research Center to H.E.G., and a fellowship from the American Diabetes Association to J.L.

ABBREVIATIONS

CEACAM1	Carcinoembryonic antigen-related cell adhesion molecule
***Ccl*$^{-/-}$**	Mice with null deletion of *Ceacam1* gene
CCL2	C-C motif chemokine ligand 2
CD3/4/8	Cluster of Differentiation 3/4/8
E-Cadherin	Epithelial cadherin
EGFR	Epidermal growth factor receptor
EMT	Epithelial-to-mesenchymal transition
FASN	Fatty acid synthase
Foxp3	Forkhead box protein P3
GAPDH	Glyceraldehyde 3-phosphate dehydrogenase
Gr1	Granulocyte receptor-1
IHC	Immunohistochemistry
Il-6	Interleukin 6
JNK	Jun N-terminal kinase
MAPK	Mitogen-activated protein kinase
PIN	Mouse prostatic intraepithelial neoplasia
PI3K	Phosphoinositide 3-kinase
PML	Promyelocytic leukemia protein
PTEN	Phosphatase and tensin homolog
Pten$^{+/+}$	Wild-type mice on the *Cc1*$^{+/+}$ background
Pten$^{+/-}$	Mice with global monoallelic deletion of *Pten*
***Pten*$^{+/-}$/*Cc1*$^{-/-}$**	Double knockout mutants
SOX9	(Sex determining region Y)-box9
SREBP-1c	Sterol regulatory element binding protein-1c
STAT3	Signal Transducer and Activator of Transcription 3
Trp53	Murine gene encoding TP53 in humans
VEGFR2	Vascular endothelial growth factor receptor 2

REFERENCES

[1]. Rubin MA, Demichelis F. The Genomics of Prostate Cancer: emerging understanding with technologic advances. Mod Pathol. 2018;31:S1–11. [PubMed: 29297493]

[2]. Chalhoub N, Baker SJ. PTEN and the PI3-kinase pathway in cancer. Annu Rev Pathol. 2009;4:127–50. [PubMed: 18767981]

[3]. Fujita K, Hayashi T, Matsushita M, Uemura M, Nonomura N. Obesity, Inflammation, and Prostate Cancer. J Clin Med. 2019;8.

[4]. McMenamin ME, Soung P, Perera S, Kaplan I, Loda M, Sellers WR. Loss of PTEN expression in paraffin-embedded primary prostate cancer correlates with high Gleason score and advanced stage. Cancer Res. 1999;59:4291–6. [PubMed: 10485474]

[5]. Deocampo ND, Huang H, Tindall DJ. The role of PTEN in the progression and survival of prostate cancer. Minerva Endocrinol. 2003;28:145–53. [PubMed: 12717346]

[6]. Grasso CS, Wu YM, Robinson DR, Cao X, Dhanasekaran SM, Khan AP, et al. The mutational landscape of lethal castration-resistant prostate cancer. Nature. 2012;487:239–43. [PubMed: 22722839]

[7]. Robinson D, Van Allen EM, Wu YM, Schultz N, Lonigro RJ, Mosquera JM, et al. Integrative clinical genomics of advanced prostate cancer. Cell. 2015;161:1215–28. [PubMed: 26000489]

[8]. Cancer Genome Atlas Research N. The Molecular Taxonomy of Primary Prostate Cancer. Cell. 2015;163:1011–25. [PubMed: 26544944]

[9]. Armenia J, Wankowicz SAM, Liu D, Gao J, Kundra R, Reznik E, et al. The long tail of oncogenic drivers in prostate cancer. Nat Genet. 2018;50:645–51. [PubMed: 29610475]

[10]. Podsypanina K, Ellenson LH, Nemes A, Gu J, Tamura M, Yamada KM, et al. Mutation of Pten/Mmac1 in mice causes neoplasia in multiple organ systems. Proc Natl Acad Sci USA. 1999;96:1563–8. [PubMed: 9990064]

[11]. Di Cristofano A, De Acetis M, Koff A, Cordon-Cardo C, Pandolfi PP. Pten and p27KIP1 cooperate in prostate cancer tumor suppression in the mouse. Nat Genet. 2001;27:222–4. [PubMed: 11175795]

[12]. Liu J, Ramakrishnan SK, Khuder SS, Kaw MK, Muturi HT, Lester SG, et al. High-calorie diet exacerbates prostate neoplasia in mice with haploinsufficiency of Pten tumor suppressor gene. Mol Metab. 2015;4:186–98. [PubMed: 25737954]

[13]. Svensson RU, Haverkamp JM, Thedens DR, Cohen MB, Ratliff TL, Henry MD. Slow disease progression in a C57BL/6 pten-deficient mouse model of prostate cancer. Am J Pathol. 2011;179:502–12. [PubMed: 21703427]

[14]. Ma X, Ziel-van der Made AC, Autar B, van der Korput HA, Vermeij M, van Duijn P, et al. Targeted biallelic inactivation of Pten in the mouse prostate leads to prostate cancer accompanied by increased epithelial cell proliferation but not by reduced apoptosis. Cancer Res. 2005;65:5730–9. [PubMed: 15994948]

[15]. Hubner A, Mulholland DJ, Standen CL, Karasarides M, Cavanagh-Kyros J, Barrett T, et al. JNK and PTEN cooperatively control the development of invasive adenocarcinoma of the prostate. Proc Natl Acad Sci USA. 2012;109:12046–51. [PubMed: 22753496]

[16]. Couto SS, Cao M, Duarte PC, Banach-Petrosky W, Wang S, Romanienko P, et al. Simultaneous haploinsufficiency of Pten and Trp53 tumor suppressor genes accelerates tumorigenesis in a mouse model of prostate cancer. Differentiation; Research in Biological Diversity. 2009;77:103–11.

[17]. Chen M, Zhang J, Sampieri K, Clohessy JG, Mendez L, Gonzalez-Billalabeitia E, et al. An aberrant SREBP-dependent lipogenic program promotes metastatic prostate cancer. Nat Genet. 2018;50:206–18. [PubMed: 29335545]

[18]. Beauchemin N, Arabzadeh A. Carcinoembryonic antigen-related cell adhesion molecules (CEACAMs) in cancer progression and metastasis. Cancer Metastasis Rev. 2013;32:643–71. [PubMed: 23903773]

[19]. Chang CL, Semyonov J, Cheng PJ, Huang SY, Park JI, Tsai HJ, et al. Widespread divergence of the CEACAM/PSG genes in vertebrates and humans suggests sensitivity to selection. PloS One. 2013;8:e61701. [PubMed: 23613906]

[20]. Lin SH, Pu YS. Function and therapeutic implication of C-CAM cell-adhesion molecule in prostate cancer. Semin Oncol. 1999;26:227–33. [PubMed: 10597733]

[21]. Busch C, Hanssen TA, Wagener C, OBrink B. Down-regulation of CEACAM1 in human prostate cancer: correlation with loss of cell polarity, increased proliferation rate, and Gleason grade 3 to 4 transition. Hum Pathol. 2002;33:290–8. [PubMed: 11979369]

[22]. Nittka S, Gunther J, Ebisch C, Erbersdobler A, Neumaier M. The human tumor suppressor CEACAM1 modulates apoptosis and is implicated in early colorectal tumorigenesis. Oncogene. 2004;23:9306–13. [PubMed: 15568039]

[23]. Tilki D, Irmak S, Oliveira-Ferrer L, Hauschild J, Miethe K, Atakaya H, et al. CEA-related cell adhesion molecule-1 is involved in angiogenic switch in prostate cancer. Oncogene. 2006;25:4965–74. [PubMed: 16568082]

[24]. Najjar SM, Russo L. CEACAM1 loss links inflammation to insulin resistance in obesity and non-alcoholic steatohepatitis (NASH). Semin Immunopathol. 2014;36:55–71. [PubMed: 24258517]

[25]. Horst AK, Najjar SM, Wagener C, Tiegs G. CEACAM1 in Liver Injury, Metabolic and Immune Regulation. Int J Mol Sci. 2018;19.

[26]. Najjar SM, Perdomo G. Hepatic Insulin Clearance: Mechanism and Physiology. Physiology (Bethesda). 2019;34:198–215. [PubMed: 30968756]

[27]. Poy MN, Yang Y, Rezaei K, Fernstrom MA, Lee AD, Kido Y, et al. CEACAM1 regulates insulin clearance in liver. Nat Genet. 2002;30:270–6. [PubMed: 11850617]

[28]. DeAngelis AM, Heinrich G, Dai T, Bowman TA, Patel PR, Lee SJ, et al. Carcinoembryonic antigen-related cell adhesion molecule 1: a link between insulin and lipid metabolism. Diabetes. 2008;57:2296–303. [PubMed: 18544705]

[29]. Ghadieh HE, Russo L, Muturi HT, Ghanem SS, Manaserh IH, Noh HL, et al. Hyperinsulinemia drives hepatic insulin resistance in male mice with liver-specific Ceacam1 deletion independently of lipolysis. Metabolism. 2019;93:33–43. [PubMed: 30664851]

[30]. Poy MN, Ruch RJ, Fernstrom MA, Okabayashi Y, Najjar SM. Shc and CEACAM1 interact to regulate the mitogenic action of insulin. J Biol Chem. 2002;277:1076–84. [PubMed: 11694516]

[31]. Abou-Rjaily GA, Lee SJ, May D, Al-Share QY, Deangelis AM, Ruch RJ, et al. CEACAM1 modulates epidermal growth factor receptor--mediated cell proliferation. J Clin Invest. 2004;114:944–52. [PubMed: 15467833]

[32]. Zalzali H, Naudin C, Bastide P, Quittau-Prevostel C, Yaghi C, Poulat F, et al. CEACAM1, a SOX9 direct transcriptional target identified in the colon epithelium. Oncogene. 2008;27:7131–8. [PubMed: 18794798]

[33]. Najjar S, Boisclair Y, Nabih Z, Philippe N, Imai Y, Suzuki Y, et al. Cloning and characterization of a functional promoter of the rat pp120 gene, encoding a substrate of the insulin receptor tyrosine kinase. J Biol Chem. 1996;271:8809–17. [PubMed: 8621519]

[34]. Leung N, Turbide C, Olson M, Marcus V, Jothy S, Beauchemin N. Deletion of the carcinoembryonic antigen-related cell adhesion molecule 1 (Ceacam1) gene contributes to colon tumor progression in a murine model of carcinogenesis. Oncogene. 2006;25:5527–36. [PubMed: 16619040]

[35]. Park JH, Walls JE, Galvez JJ, Kim M, Abate-Shen C, Shen MM, et al. Prostatic intraepithelial neoplasia in genetically engineered mice. Am J Pathol. 2002;161:727–35. [PubMed: 12163397]

[36]. Robinson MR, Thomas BS. Effect of hormonal therapy on plasma testosterone levels in prostatic carcinoma. Br Med J. 1971;4:391–4. [PubMed: 5124437]

[37]. Sarker D, Reid AH, Yap TA, de Bono JS. Targeting the PI3K/AKT pathway for the treatment of prostate cancer. Clin Cancer Res. 2009;15:4799–805. [PubMed: 19638457]

[38]. Thomsen MK, Ambroisine L, Wynn S, Cheah KS, Foster CS, Fisher G, et al. SOX9 elevation in the prostate promotes proliferation and cooperates with PTEN loss to drive tumor formation. Cancer Res. 2010;70:979–87. [PubMed: 20103652]

[39]. Zhou L, Yu Y, Sun S, Zhang T, Wang M. Cry 1 Regulates the Clock Gene Network and Promotes Proliferation and Migration Via the Akt/P53/P21 Pathway in Human Osteosarcoma Cells. J Cancer. 2018;9:2480–91. [PubMed: 30026846]

[40]. Cano A, Perez-Moreno MA, Rodrigo I, Locascio A, Blanco MJ, del Barrio MG, et al. The transcription factor snail controls epithelial-mesenchymal transitions by repressing E-cadherin expression. Nat Cell Biol. 2000;2:76–83. [PubMed: 10655586]

[41]. Shi J, Wang L, Zou C, Xia Y, Qin S, Keller E, et al. Tumor microenvironment promotes prostate cancer cell dissemination via the Akt/mTOR pathway. Oncotarget. 2018;9:9206–18. [PubMed: 29507684]

[42]. Currie E, Schulze A, Zechner R, Walther TC, Farese RV Jr., Cellular fatty acid metabolism and cancer. Cell Metab. 2013;18:153–61. [PubMed: 23791484]

[43]. Datta D, Aftabuddin M, Gupta DK, Raha S, Sen P. Human Prostate Cancer Hallmarks Map. Sci Rep. 2016;6:30691. [PubMed: 27476486]

[44]. Galbraith L, Leung HY, Ahmad I. Lipid pathway deregulation in advanced prostate cancer. Pharmacol Res. 2018;131:177–84. [PubMed: 29466694]

[45]. Wong JT, Kim PT, Peacock JW, Yau TY, Mui AL, Chung SW, et al. Pten (phosphatase and tensin homologue gene) haploinsufficiency promotes insulin hypersensitivity. Diabetologia. 2007;50:395–403. [PubMed: 17195063]

[46]. Ghosh S, Kaw M, Patel PR, Ledford KJ, Bowman TA, McLnerney MF, et al. Mice with null mutation of Ceacam I develop nonalcoholic steatohepatitis. Hepat Med: Res Evidence. 2010;2010:69–78.

[47]. Korsten H, Ziel-van der Made AC, van Weerden WM, van der Kwast T, Trapman J, Van Duijn PW. Characterization of Heterogeneous Prostate Tumors in Targeted Pten Knockout Mice. PloS One. 2016;11:e0147500. [PubMed: 26807730]

[48]. Dankner M, Gray-Owen SD, Huang YH, Blumberg RS, Beauchemin N. CEACAM1 as a multi-purpose target for cancer immunotherapy. Oncoimmunology. 2017;6:e1328336. [PubMed: 28811966]

[49]. Abrams SI, Netherby CS, Twum DY, Messmer MN. Relevance of Interferon Regulatory Factor-8 Expression in Myeloid-Tumor Interactions. J Interferon Cytokine Res. 2016;36:442–53. [PubMed: 27379866]

[50]. Dror N, Rave-Harel N, Burchert A, Azriel A, Tamura T, Tailor P, et al. Interferon regulatory factor-8 is indispensable for the expression of promyelocytic leukemia and the formation of nuclear bodies in myeloid cells. J Biol Chem. 2007;282:5633–40. [PubMed: 17189268]

[51]. Wang S, Gao J, Lei Q, Rozengurt N, Pritchard C, Jiao J, et al. Prostate-specific deletion of the murine Pten tumor suppressor gene leads to metastatic prostate cancer. Cancer Cell. 2003;4:209–21. [PubMed: 14522255]

[52]. Ahmad I, Mui E, Galbraith L, Patel R, Tan EH, Salji M, et al. Sleeping Beauty screen reveals Pparg activation in metastatic prostate cancer. Proc Natl Acad Sci U S A. 2016;113:8290–5. [PubMed: 27357679]

[53]. Arabzadeh A, Dupaul-Chicoine J, Breton V, Haftchenary S, Yumeen S, Turbide C, et al. Carcinoembryonic Antigen Cell Adhesion Molecule 1 long isoform modulates malignancy of poorly differentiated colon cancer cells. Gut. 2016;65:821–9. [PubMed: 25666195]

[54]. Wegwitz F, Lenfert E, Gerstel D, von Ehrenstein L, Einhoff J, Schmidt G, et al. CEACAM1 controls the EMT switch in murine mammary carcinoma in vitro and in vivo. Oncotarget. 2016;7:63730–46. [PubMed: 27572314]

[55]. Yang X, Lin Y, Shi Y, Li B, Liu W, Yin W, et al. FAP Promotes Immunosuppression by Cancer-Associated Fibroblasts in the Tumor Microenvironment via STAT3-CCL2 Signaling. Cancer Res. 2016;76:4124–35. [PubMed: 27216177]

[56]. Su W, Han HH, Wang Y, Zhang B, Zhou B, Cheng Y, et al. The Polycomb Repressor Complex 1 Drives Double-Negative Prostate Cancer Metastasis by Coordinating Stemness and Immune Suppression. Cancer Cell. 2019;36:139–55 e10. [PubMed: 31327655]

[57]. Zhang Z, La Placa D, Nguyen T, Kujawski M, Le K, Li L, et al. CEACAM1 regulates the IL-6 mediated fever response to LPS through the RP105 receptor in murine monocytes. BMC Immunol. 2019;20:7. [PubMed: 30674283]

[58]. Lin DL, Whitney MC, Yao Z, Keller ET. Interleukin-6 induces androgen responsiveness in prostate cancer cells through up-regulation of androgen receptor expression. Clin Cancer Res. 2001;7:1773–81. [PubMed: 11410519]

[59]. Flammiger A, Weisbach L, Huland H, Tennstedt P, Simon R, Minner S, et al. High tissue density of FOXP3+ T cells is associated with clinical outcome in prostate cancer. Eur J Cancer. 2013;49:1273–9. [PubMed: 23266046]

[60]. Rueckschloss U, Kuerten S, Ergun S. The role of CEA-related cell adhesion molecule-1 (CEACAM1) in vascular homeostasis. Histochem Cell Biol. 2016;146:657–71. [PubMed: 27695943]

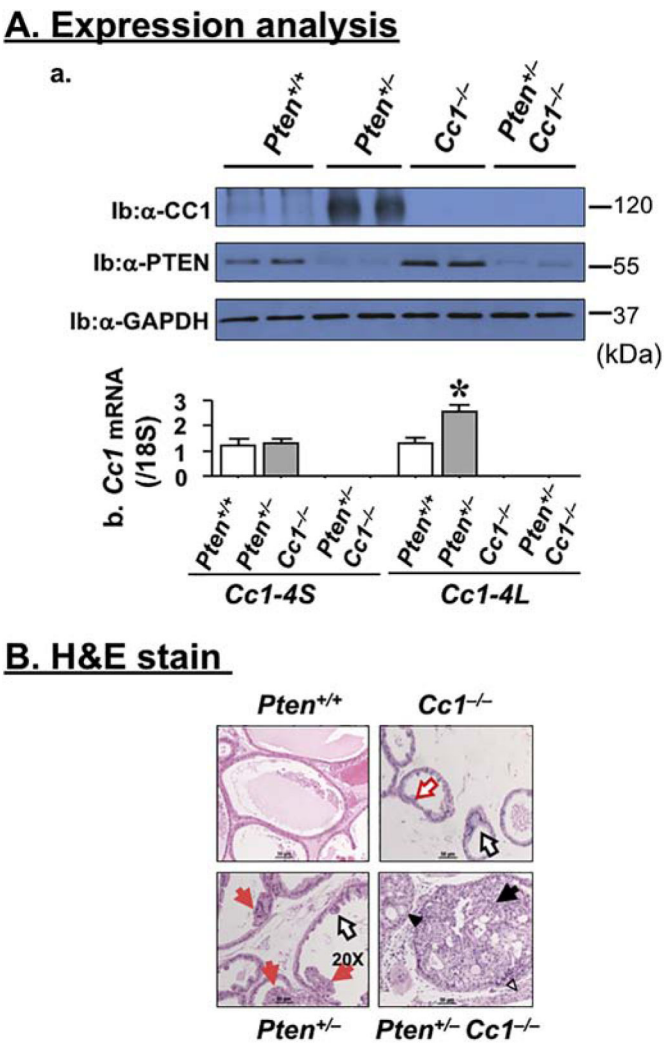

Figure 1. Null mutation of *Ceacam1* gene causes neoplastic progression in *Pten*$^{+/-}$ prostates.

(A.*a*) Gels were applied in parallel and Western blot analysis of protein lysates from 2 mice/genotype was carried out by immunoblotting (Ib) with polyclonal antibodies against CEACAM1 (α-CC1) and PTEN (α-PTEN). The lower half of the CEACAM1 gel was used to immunoblot with α-GAPDH monoclonal antibody for normalization. (A.*b*) qRT-PCR analysis of the mRNA encoding the long (*Cc1–4L*) and the short (*Cc1–4S*) isoforms of CEACAM1, normalized to 18S in duplicate. Data were analyzed by one-way ANOVA with Tukey's for multiple comparisons and values expressed as mean ± SEM (n=3–4/genotype). **P*<0.05 vs *Pten*$^{+/+}$ wild-types. (B) Ventral and dorsolateral lobes of the prostate from seven-month old mice were stained by H&E for histological analysis. The most progressive PIN from each group was counted. *Pten*$^{+/+}$ show normal glandular structure. *Cc1*$^{-/-}$ show mostly features of PIN-I (hollow red arrow) and PIN-II (hollow black arrow). *Pten*$^{+/-}$ exhibit predominantly PIN-III with extensive gland-in-gland proliferation inside the lumen (solid red arrow). *Pten*$^{+/-}$/*Cc1*$^{-/-}$ develop PIN-IV with increasing complexity of glandular proliferation (solid black arrowhead), carcinoma in situ (solid black arrow) and a diffuse stromal invasion (hollow black arrowhead). Arrows and arrowheads are pointing to a few

examples of each PIN grade for simplicity. Panels represent at least 13 mice per group, per Table 1. Magnification: 50μm (20X).

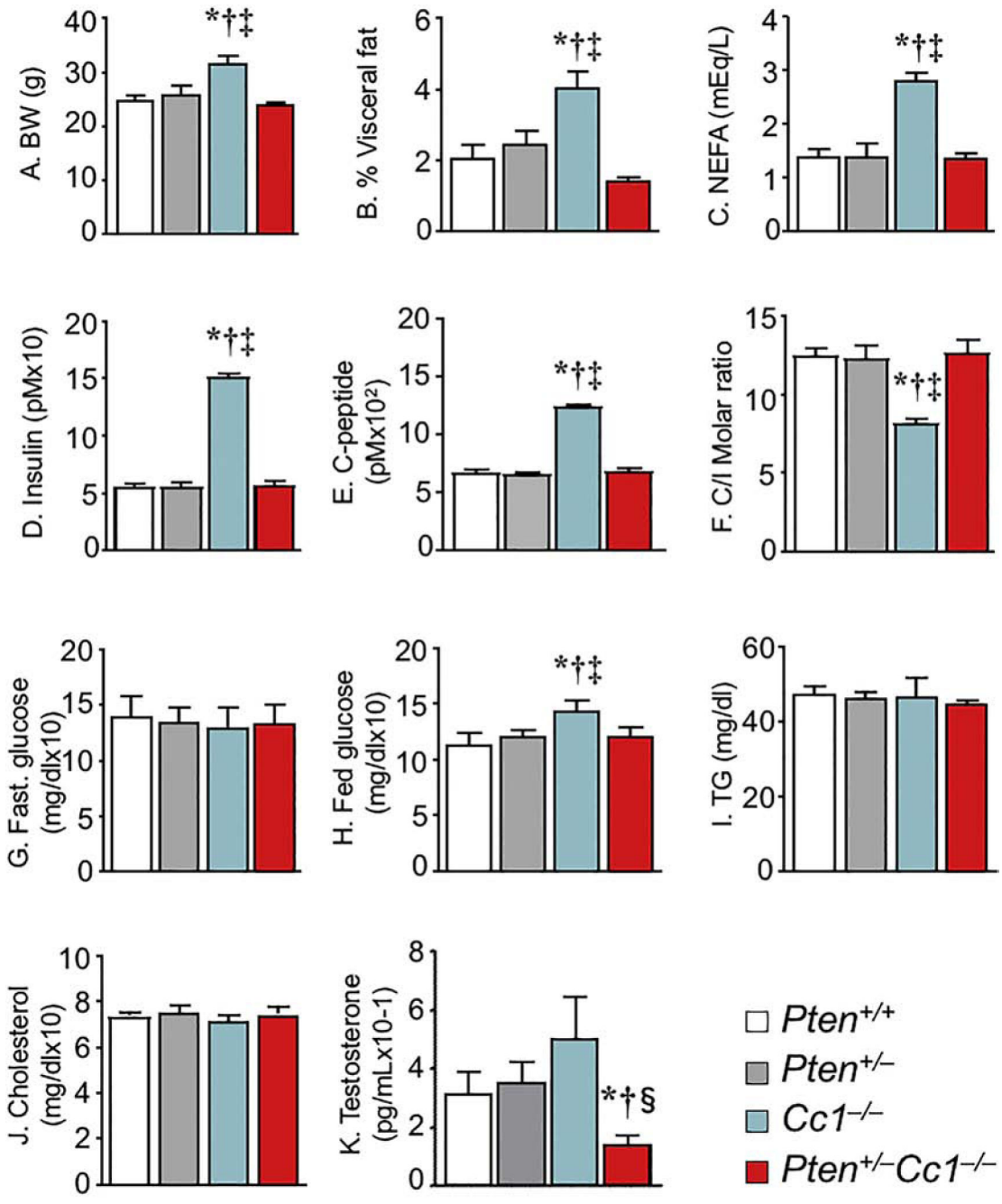

Figure 2. Metabolic parameters.

Mice (7 months of age, n=8–15/each genotype) were fasted overnight and their blood was drawn at 11:00 a.m. the next morning to process steady-state plasma levels, except for fed blood glucose when blood was drawn at 10:00 p.m. from *ad libitum* fed mice. Visceral adiposity was expressed as % of gonadal plus inguinal white adipose tissue per total body mass. Insulin clearance was determined as molar ratio of steady-state plasma C-peptide/ Insulin (C/I). Data were analyzed by one-way ANOVA with Tukey's for multiple comparisons and values were expressed as mean ± SEM. *P<0.05 vs *Pten*$^{+/+}$, †P<0.05 vs *Pten*$^{+/-}$, ‡P<0.05 vs *Pten*$^{+/-}$ *Cc1*$^{-/-}$, §P<0.05 vs *Cc1*$^{-/-}$.

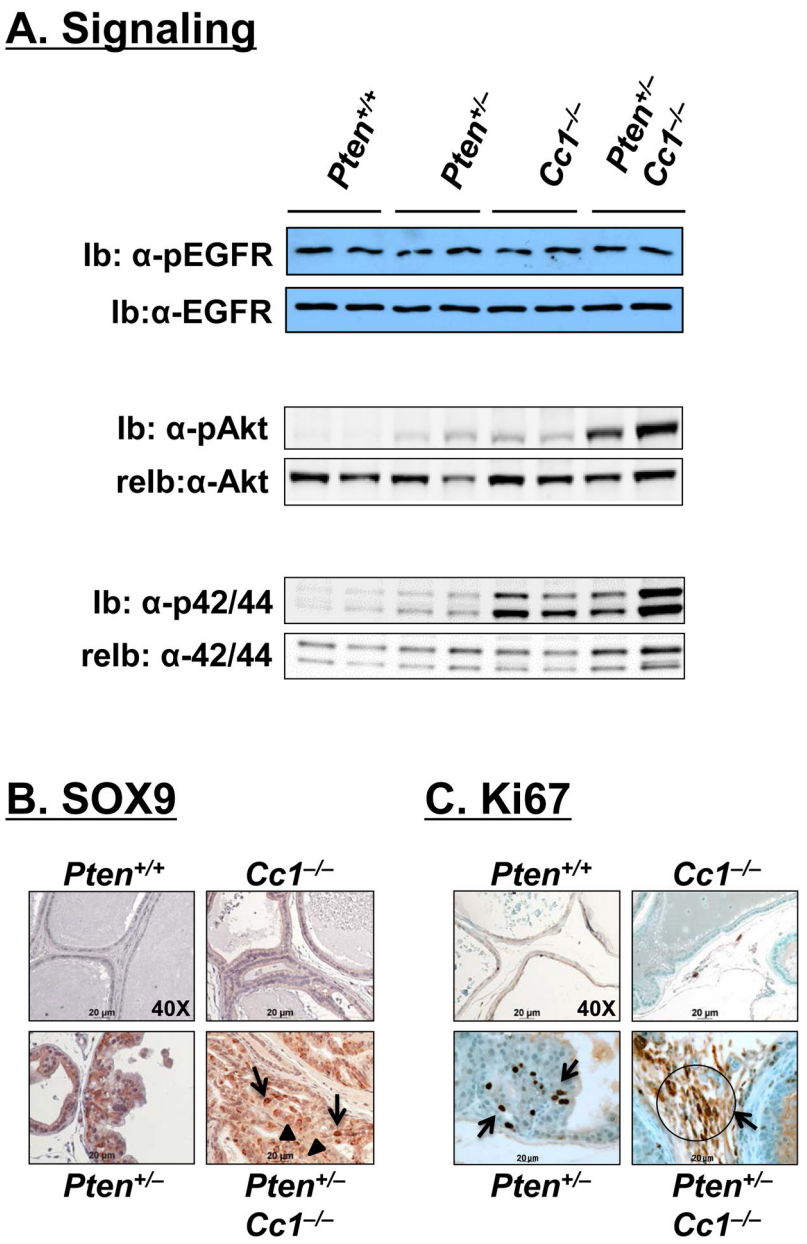

Figure 3. Null mutation of *Ceacam1* gene induces cell proliferation in *Pten*$^{+/-}$ prostates.

(A) Proteins from prostates of mice (7 months of age, n=2 mice/genotype) were analyzed by Western blot in parallel gels using antibodies against either phosphorylated or total proteins for immunoblotting (Ib) to detect signaling through EGFR (a), Akt (b) and p42/p44 (MAPK) (c). (B) Immunohistochemical (IHC) analysis of SOX9 with arrows pointing to nuclear and arrowheads to cytoplasmic staining (only few were highlighted for simplicity). (C) Ki67 immunostaining with arrows pointing to a group of stained cells within a circle for simplicity (n≥5/group). Magnification: 20µm (40X).

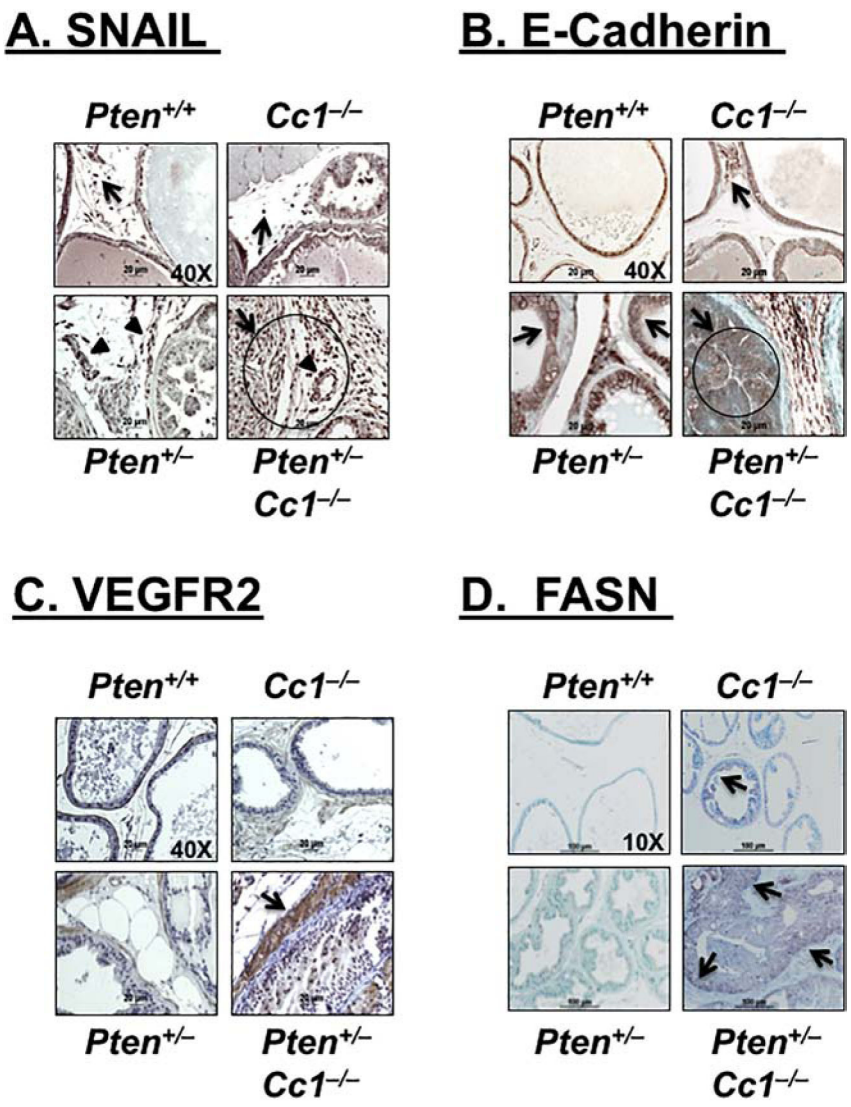

Figure 4. Null deletion of *Ceacam1* gene induces epithelial-to-mesenchymal transition, angiogenesis and lipogenesis in *Pten*$^{+/-}$ prostates.

(A) IHC analysis with α-SNAIL antibody. Arrows refer to sporadic cells or a group of cells within a circle for simplicity. Arrowheads point to staining along the lining of vessels. (B) IHC analysis to detect E-Cadherin (arrows). Circle highlights repressed E-Cadherin expression by SNAIL (C) IHC analysis with α-VEGFR2, an angiogenesis marker, and (D) with α-FASN, a lipogenesis marker. Arrows refer to few of the immunopositive cells. All were at n≥5/group and at magnification of 20μm (40X), except for α-FASN, which was at 100μm (10X).

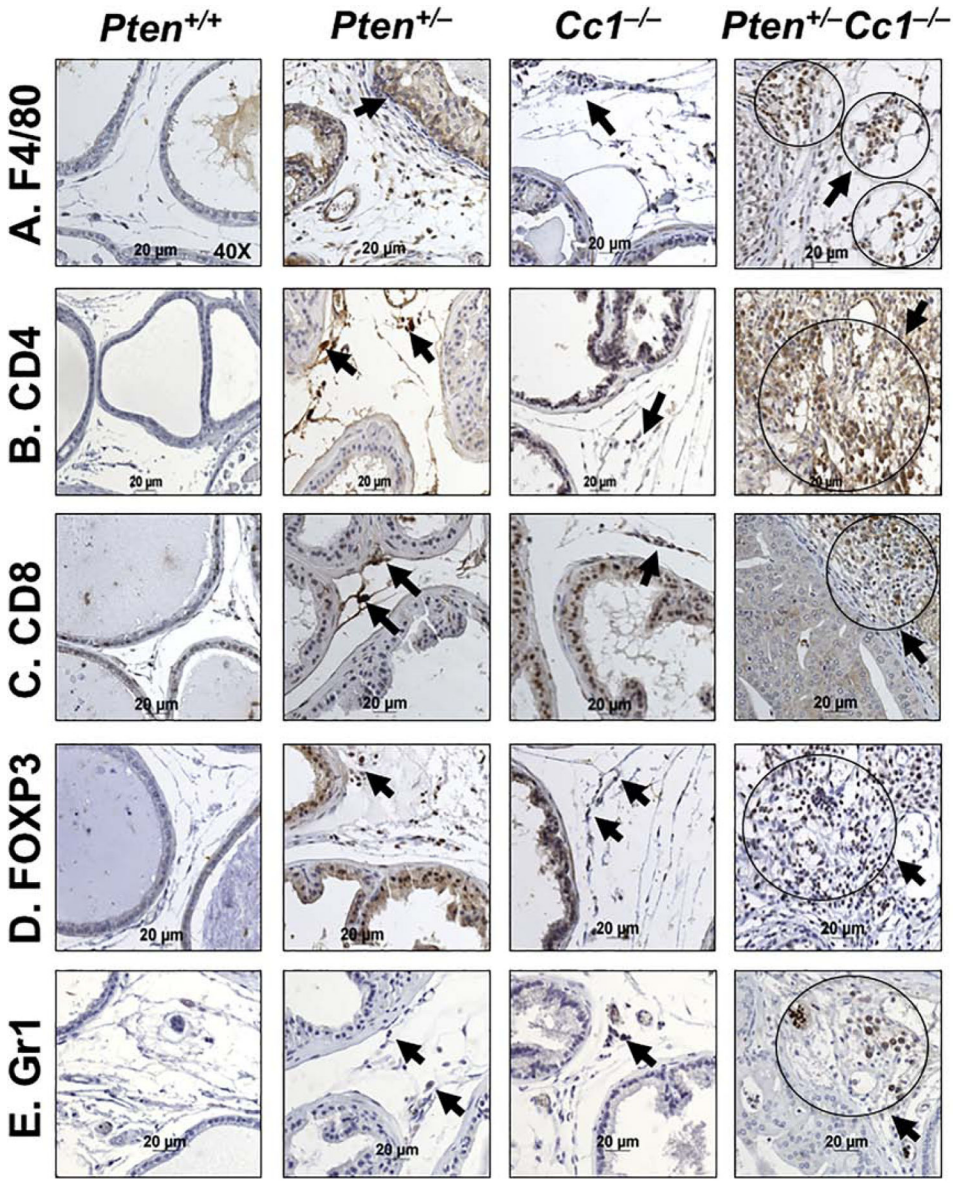

Figure 5. Null deletion of *Ceacam1* gene induces inflammation in *Pten*$^{+/-}$ prostates.

Immunohistochemical analyses of F4/80, CD4, CD8, FoxP3 and Gr1-R (n≥5/group). All exposures shown are at 20μm (40X) magnification. As above, circles in the double mutants indicate a group of immunopositive cells, as opposed to individual mutants where arrows point to few sporadic positive cells.

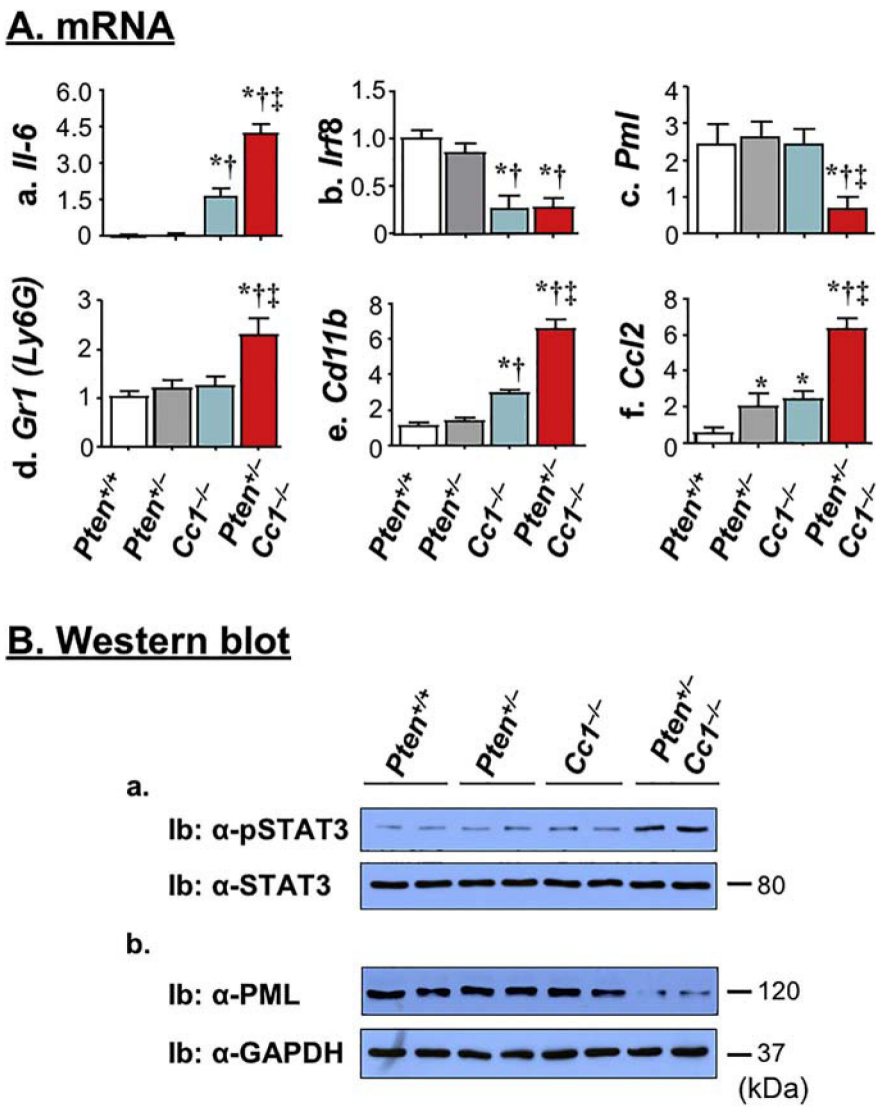

Figure 6. Null deletion of Ceacam1 causes a reduction in PML levels in *Pten*$^{+/-}$ prostates.

(A) As in Table 2, mRNA levels from prostates of mice at 7 months of age (n=3–4/genotype) were analyzed by qRT-PCR normalized to 18S in triplicate using gene-specific oligos. Data were analyzed by one-way ANOVA with Tukey's for multiple comparisons and values were expressed as mean ± SEM. *P<0.05 vs *Pten*$^{+/+}$, †P<0.05 vs *Pten*$^{+/-}$, ‡P<0.05 *Pten*$^{+/-}$/*Cc1*$^{-/-}$ vs *Cc1*$^{-/-}$ mice. *Il-6*: Interleukin-6; *Irf8*: Interferon regulatory factor; *Pml*: Promyelocytic leukemia; *Gr-1*: Granulocyte receptor-1; *CD-11b*: Cluster of differentiation-11b; *Ccl2*: CCL2 C-C motif chemokine ligand 2. (B) Proteins from prostates of mice (n=2 mice/genotype) were analyzed by immunoblotting (Ib) using antibodies against α-phopho-STAT3 in parallel to α-STAT3 (a) or α-PML (upper half) and α-GAPDH (lower half) of the same gel for normalization (b).

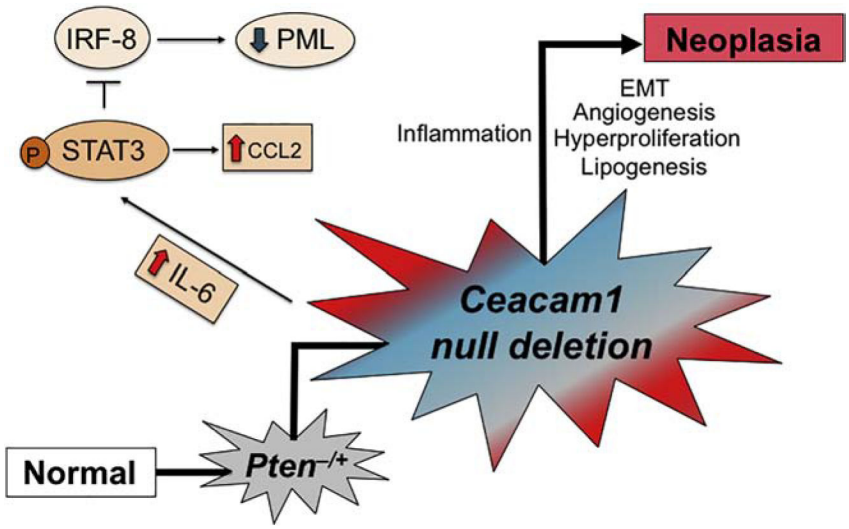

Figure 7.

Deleting *Ceacam1* gene advances prostate neoplasia in *Pten* haploinsuffiicent mice by activating IL6/STAT3 inflammatory pathways and inducing lipogenesis.

Table 1.

PIN progression in mice with *Ceacam1* and *Pten* mutations

	***Pten*$^{+/+}$ (n=24)**	***Pten*$^{+/-}$ (n=13)**	***Ccl*$^{-/-}$ (n=26)**	***Pten*$^{+/-}$/*Ccl*$^{-/-}$ (n=19)**
PIN-I	33 (8)	0	46 (12)	0
PIN-II	58 (14)	15 (2)	50 (13)	16 (3)
PIN-III	8 (2)	69 (9)	4 (1)	42 (8)
PIN-IV	0	15 (2)	0	32 (6)
Carcinoma	0	0	0	10 (2)

Ventral and dorsolateral lobes of the prostate were excised from *Pten*$^{+/+}$, *Pten*$^{+/-}$, *Cc1*$^{-/-}$, and *Pten*$^{+/-}$/*Cc1*$^{-/-}$ mice (7-month old; total number 13–26). PIN lesions were scored in H&E stained sections by at least 2 certified pathologists. Values in each PIN group represent a percentage per total mice examined and numbers in parentheses represent absolute number of mice. PIN: Mouse prostatic intraepithelial neoplasia

Table 2.

mRNA analysis of genes involved in cell proliferation, angiogenesis, lipogenesis and inflammation

	Pten$^{+/+}$	*Pten*$^{+/-}$	*Ccl*$^{-/-}$	*Pten*$^{+/-}$/*Ccl*$^{-/-}$
Cell proliferation				
Sox9	2.5 ± 0.2	5.9 ± 0.2 *	2.9 ± 0.2	10.3 ± 0.2 *†‡
β-Catenin	1.5 ± 0.2	6.6 ± 1.6 *	1.5 ± 0.3	19.3 ± 0.6 *†‡
Cyclin D	0.9 ± 0.1	2.7 ± 0.3 *	0.8 ± 0.4	4.0 ± 0.8 *†
p21	1.6 ± 0.4	8.7 ± 0.9 *	1.6 ± 0.1	66.4 ± 5.6 *†‡
Igf-1	0.5 ± 0.0	0.6 ± 0.1	0.6 ± 0.0	0.9 ± 0.2 *†‡
Angiogenesis				
Hif-lα	1.4 ± 0.4	7.0 ± 1.1 *	1.9 ± 2.0	22.8 ± 0.3 *†‡
Ang-1	1.2 ± 0.1	2.7 ± 0.5 *	0.9 ± 0.2	6.5 ± 0.5 *†‡
Lipogenesis				
Srebp-lc	1.5 ± 0.2	3.0 ± 0.6 *	2.2 ± 0.8	6.6 ± 0.8 *†‡
Ppary	0.8 ± 0.1	8.5 ± 1.3 *	0.6 ± 0.1	35.3 ± 2.9 *†‡
Inflammation				
Tnfa	0.8 ± 0.2	11.6 ± 1.7 *	2.1 ± 0.7	27.3 ± 5.1 *†‡
Cd3	0.9 ± 0.2	2.7 ± 0.6 *	1.3 ± 0.2	11.1 ± 1.6 *†‡
Cd45	1.9 ± 0.4	19.2 ± 3.9 *	5.5 ± 1.2 *	35.8 ± 5.7 *†‡
Foxp3	1.0 ± 0.2	1.6 ± 0.2	0.9 ± 0.4	3.5 ± 0.3 *†‡
Ifnγ	1.8 ± 0.5	2.4 ± 0.3	8.6 ± 0.4 *†	1.8 ± 0.0‡
Irf1	1.2 ± 0.1	1.5 ± 0.1	4.4 ± 1.0 *†	0.9 ± 0.3‡
Ir/3	1.5 ± 0.2	1.7 ± 0.1	8.8 ± 0.3 *†	1.8 ± 0.1‡
Il-4	5.7 ± 1.2	6.2 ± 0.5	30.6 ± 2.9 *†	7.7 ± 0.4‡
Il-13	1.9 ± 0.6	1.8 ± 0.2	13.1 ± 3.1 *†	1.6 ± 0.6‡

Mice (7 months of age, n=3–4/genotype). Prostate extracts were analyzed by qRT-PCR normalized to 18S in triplicate using gene-specific oligos. Values are expressed as mean ± SEM.

*P<0.05 vs *Pten*$^{+/+}$,

†P<0.05 vs *Pten*$^{+/-}$,

‡P<0.05 *Pten*$^{+/-}$/*Cc1*$^{-/-}$ vs *Cc1*$^{-/-}$ mice.

Sox9: (Sex determining region Y)-box9; *p21*: cyclin-dependent kinase (CDK) inhibitor p21; *Igf-1:* Insulin like growth factor-1; *Hif1α*: Hypoxia Inducible Factor 1α; *Ang1*: Angiopoietin1; *Srebp-1c*: Sterol regulatory element binding protein-1c; *Pparγ*: Peroxisome proliferator-activated receptor γ; *Tnfa*: Tumor necrosis factor alpha*; Cd3/45*: Cluster of Differentiation 3/45; *Foxp3*: Forkhead box protein P3; *Ifnγ*: Interferon γ, *Irf1/3*: Interferon regulatory factor; *Il-4/13*: interleukin 4/13.